Analyst

Accepted Manuscript

ROYAL SOCIETY OF CHEMISTRY

www.rsc.org/analyst

Analyst

ARTICLE

Electrochemical DNA sensor Based on Polyaniline/graphene: High Sensitivity to DNA Sequences in a Wide Range

Received 00th January 20xx,
Accepted 00th January 20xx

DOI: 10.1039/x0xx00000x

www.rsc.org/

Qing Zheng[a♀], Hao Wu[a♀], Zongxu Shen[a♀], Wenyu Gao[a♀], Yu Yu[a], Yuehui Ma[b], Weijun Guang[b], Quangui Guo[c], Rui Yan[c], Junzhong Wang[c]*, Kejian Ding[a]*

A free-label electrochemical DNA sensor was fabricated by deposition of polyaniline and pristine graphene nanosheet (P/G_{ratios}) composites in different mass ratios, probe DNA and bovine serum albumin (BSA) layer by layer on the surface of glassy carbon electrode (GCE). Electrochemical impedance spectroscopy (EIS) was employed to monitor every step of fabrication of P/G_{ratios}-based DNA sensors and to evaluate the detection results in terms of the hybridization of complementary DNA, mutation DNA and non-complementary DNA. The results illustrate that the P/G_{ratios}-based DNA sensor could high efficiently detect complementary DNA from 0.01 pm to 1 μm and discriminate single-nucleotide polymorphisms (SNPs). In the process of detection, double-stranded DNA (dsDNA), resulted from hybridization of probe DNA, escaping from or remaining on the sensor surface, was monitored by changing the ratio of polyaniline (PANI) to graphene, which was decided by the competition between electrostatic interaction and Brownian motion.

Introduction

Electrochemical DNA sensors have received intense attention recently owing to several reasons.[1-4] Firstly, simple portable DNA detection tools are highly demanded in early cancer diagnosis and the development of genetically modified organisms.[5,6] Secondly, electrochemical signaling methods involved in DNA sensors are simple, sensitive, specific and cost-effective.[7-9] Thirdly, aptamers are short single-stranded oligonucleotides being able to recognize and bind to specific targets.[10] They are analogous to antibodies but possess several advantages including wider recognition range of targets, higher affinity, easier synthesis and modification.[11] A lot of works have studied the immobilization of aptamers on the surfaces of various electrodes including Au,[12] carbon nanotube,[13] nanodiamond,[14] reduced graphene oxide[15] and conjugated polymer.[16] However, electrochemical DNA sensors are still limited in sensitivity, stability, and cost of fabrication.[17]

In the research of how to fabricate economic and functional DNA sensors, graphene quickly came to the attention of many scientists and researchers.[18,19] As a kind of two-dimensional material of sp^2 bonded atomic carbon with long-range π cloud, graphene is of planar surface, high electrical and thermal conductivity, strong mechanical strength and good biocompatibility.[20,21] In addition, graphene is good at adsorbing and sensing single-stranded DNA (ssDNA).[22-24] All these make graphene a kind of promising material for applications in biosensors,[25,26] especially the fabrication of electrochemical DNA sensors because ssDNA would be stably immobilized on the surface of graphene through π-π stacking interaction between the conjugated π bonds of nucleotide bases and the hexagonal units of graphene.[27] In a DNA biosensor, the immobilized-probe DNA selectively hybridizes with target DNA and the whole process of hybridization is monitored by electrochemical impedance spectroscopy (EIS) in the form of the change of charge transfer resistance (R_{ct}).[28] Seemingly, the ending of hybridization would bring about the decrease of R_{ct} value in the result of double-stranded DNA (dsDNA, in the presence of target/probe DNA) escaping from the surface of biosensor, which is witnessed by many of researchers and their experiments.[29,30] However, some researchers oppositely suggested that the dsDNA still remain on the surface of biosensor leading to the raise of impedemetric value.[31,32] This dispute on scientific facts interests us so much that we set off to make efforts to comb scientific reasons behind these conflicting facts and look forward to contributing to the improvement of electrochemical DNA sensors.

It turns out to be not easy to realize this goal when the researchers firstly met with the limitations of recent DNA sensors which are built on the basis of reduced graphene oxide that lacks of the native properties of graphene owing to many defects.[33] Fortunately, Wang et al succeeded in preparing pristine few-layer graphene flakes through electrochemical exfoliation of graphite at high yield.[34] These graphene flakes exhibit higher sensitivity to ssDNA than surface-enhanced laser

[a] College of Life sciences and Bioengineering, Beijing Jiaotong University, Beijing 100044, P R China.
[b] Key Laboratory of Carbon Materials, Institute of Coal Chemistry, Chinese Academy of Science, Taiyuan, 030001, P R China.
[c] Institute of Animal Sciences, Chinese Academy of Agricultural Sciences, Beijing 100083, P R China.
† ♀ These authors have equal contribution to this work.
Electronic Supplementary Information (ESI) available: [more XRD,AFM,UV-Vis,SEM,Scheme images are Included]. See DOI: 10.1039/x0xx00000x

desorption/ionization-mass spectrometry technique.[35] In the meantime, the new technique also largely reduces the fabrication cost of graphene electrodes so provides great chance to produce such electrodes on a large scale.[34,35] Except the invaluable improvement, however, we found that graphene-flakes are problematic because they are rarely able to remain on electrodes in DNA water solution which would lead to serious impact on the stability of the sensors and the accuracy of their results. To solve this problem, we introduced conductive polymer polyaniline,[36] an excellent organic conductor with charges, to "stick" graphene flakes on glassy carbon electrodes (GCE). Polyaniline involves outstanding environmental stability and biocompatibility, which also endowed polyaniline's popularity in the exploitation of biosensors,[37,38] especially the DNA sensors.[39,40] Thus, it is possible for researchers to build a new biosensing platform for impedance responses to target DNA oligomer by depositing pristine graphene flakes and charged polyaniline on GCE in sequence.

To avoid the non-specific adsorption of the target DNA, we further modified electrodes with bovine serum albumin (BSA) as an auxiliary medium, and probed into the interaction between probe DNA and target DNA with help of EIS analyzing the developed sensor's sensing ability in terms of its impedance response in the presence of $K_{3/4}[Fe(CN)_6]$ solution.

When it comes to the conclusion, we found that the two parties suggesting opposite results should not blame to each other because both of them are partially right since the impedance response of the DNA sensor is actually dynamic depending on the mass proportion of polyaniline and graphene.[29-32] To be clearer, we found out that the response is directly related to the mass proportion of polyaniline and graphene. We proposed that the linear increasing response of charge transfer resistance should result from dsDNA's remaining on the surface of the platform with much polyaniline while the linear decreasing response should be assigned to dsDNA's releasing off the sensor with dominative graphene.

Experimental

Apparatus and chemicals

Electrochemical impedance spectroscopy measurements were carried out in CHI660E electrochemical work station (CHI instrument, Austin, TX, USA). A glassy carbon electrode (GCE) was employed as the working electrode, a platinum wire as the counter electrode and an Ag/AgCl electrode with a saturated KCl solution as the reference electrode. The work area of GCE was 7.065 mm^2. Scanning electron microscope (SEM) and transmission electron microscope (TEM) were performed on a JSM-7001F FESEM (Field emission scanning electron microscopy) and a JEM- 2100F microscope at an acceleration voltage of 200 kV, respectively. All of synthetic oligonucleotides were purchased from Beijing Biomedical Co., Ltd (Beijing, China).The sequences of oligonucleotides are listed in Table 1.

Stock solutions of the oligonucleotides were diluted with TE buffer (10 mM Tris-HCl, 1 mM EDTA, pH=8.0). Propylene carbonate (PC, anhydrous, 99%), lithium perchlorate ($LiClO_4$, 99.8%, powder), lithium chloride (LiCl, 99%), hydrochloric acid (HCl, ~37%), ethanol (C_2H_6O, 99.8%), ammonia (28%), Tetramethylammonium hydroxide（TMA, aqueous, 25wt%） and N,N-dimethylformamide (DMF) were purchased from Aladdin (Shanghai, China). The graphite powder (the average particle size < 30 μm) was purchased from Xianfeng Nanotechnology Co., Ltd (Nanjing, China). Polyaniline, in the form of emeraldine salt was purchased from Jianya New Material technology co., Ltd (Shijiazhuang, China), and the number of aniline repeat units is ~480, which is measured by light scattering. All chemicals were used with no further purification. Water (18.2 MΩ cm^{-1}) used in the experiments was generated by a Milli-Q water-purification system (Millipore, Bedford, MA, USA).

Synthesis of pristine graphene flakes

Graphene flakes were obtained by electrochemical expansion of graphite lithium perchlorate in propylene carbonate electrolyte.[34] Graphite powder (5 g) in a porous plastic tube (PPT) with aluminum wire was used as negative electrode and carbon rod as positive electrode. The working solvent was 30 mg/mL of $LiClO_4$ in propylene carbonate (PC) and high potential of 10 V was adopted in order to activate Li/PC co-intercalation in graphite. After full electrochemical charging, the graphite powder was expanded and transferred from PPT to a glass Suslick cell (15 mL). The expanded graphite was sonicated for 15 hours in concentrated 50 mg/mL of LiCl in DMF (10 mL), PC (2 mL) and TMA (1 mL) solution. And then the above intermixture was washed with HCl/DMF and Millipore water several times.[34] Finally, graphene powder was collected after drying at 80°C.

Fabrication of Polyaniline/Pristine Graphene flake Composites under various mass ratios (P/G_{ratios})

The composites of polyaniline and graphene flakes were

Table 1. Sequences of all oligonucleotides

Single stranded DNA names	Sequences
Probe DNA	GCTCTAGAGCGGTTGGTGTGGTTGGTTTTTTTTTT (3'- 5')
Complementary DNA (Target DNA)	CGAGATCTCGCCAACCACACCAACCAAAAAAAAAA (5'- 3')
Mutant DNA	CGAGATCTCGCCAAC**G**ACACCAACCAAAAAAAAAA (5'- 3')
non-complementary DNA	TAGTCCTGTGGTGGTTGAGTGGATACCCCCCCCCC (5'- 3')

synthesized by mixing graphene dispersion and polyaniline dispersion in water with the assist of bath sonication. The composites of polyaniline (P) and graphene (G) with different mass ratios are signed as P/G_{ratios}. For example, $P/G_{1:100}$ is the composite of polyaniline and graphene with the mass ratio of 1/100. Typically, 1:1, 1:2, 1:10, 1:20 and 1:100 of P/G composites were synthesized, respectively. After mixing polyaniline and graphene flakes, the mixtures were sonicated for more than 8 hours with the help of an ultrasonic cleaner to improve the uniformity and dispersion.

GCE-P/G electrode fabrication through GCE modification with P/G composites

A glassy carbon electrode (GCE, 3.0 mm in diameter, Gauss Union) was polished with alumina slurry to obtain a mirror-like surface and then activated in 0.05 M H_2SO_4 by cycling the potential from 0 to 2.0 V (vs. Ag/AgCl, sat. KCl) at a scanning rate of 50 mV/s. The activated GCE was washed with a copious amount of Millipore water and then dried with N_2 gas. Then 2.5 µL of above prepared P/G_{ratio} composites were dropped and expanded into P/G_{ratio} film on the surface of GCE. Finally, the GCE-P/G_{ratio} electrode was washed with Millipore water several times and dried with N_2 gas.

Immobilization of Probe DNA and BSA conjugation to the GCE-P/Gelectrode (the sensor GCE-P/G-Probe)

The probe oligonucleotide was dissolved in TE buffer to obtain a $1e^{-5}$ M solution. 2.5 µL of the Probe DNA solution was deposited on the GCE-P/G_{ratios} and dried with N_2 gas for 4 h at room temperature. Afterwards, the GCE-P/G_{ratios} immobilized with probe DNA electrode (GCE-P/G_{ratios}-Probe DNA) was gently washed with Millipore water to remove excess and non-immobilized Probe DNA. The electrode of GCE-P/G_{ratios} immobilized with probe DNA was immersed in bovine serum albumin (BSA) solution for 2 hours to realize BSA conjugation at room temperature. Then, the electrode was washed with Millipore water. Finally, the DNA sensor (GCE-P/G_{ratios}-Probe, that is, GCE-P/G_{ratios} DNA sensor), modified by BSA, was collected for next-step target DNA hybridization.

Hybridization of target DNA to the sensor GCE-P/G-probe

Before electrochemical impedance spectroscopy measurements, the GCE-P/G_{ratios}-Probe were incubated in 300 µL of 2X SSC buffer containing target DNA with different concentrations at 42 °C for 20 mins to allow target DNA molecules completely to hybridize with the probe oligonucleotides.[30] After being washed with Millipore water thoroughly, the electrode named GCE-P/G-probe-target was collected for EIS analysis. The pUC19 DNA, a circular double stranded DNA with 2686 base pairs, was extracted from the competent cells. The extracted DNA was cut into linear DNA molecule by enzyme digestion. After that, the DNA samples were denatured by heating at 95 °C for 10 mins and applied ice shock for 1 min after heating. Finally, the samples were collected for hybridization.

Electrochemical impedance spectroscopy measurements

All Electrochemical Impedance Spectroscopy (EIS) measurements were made in an electrochemical cell containing 3.5% NaCl, 10 mM $K_3[Fe(CN)_6]$ and $K_4[Fe(CN)_6]$. Faradic impedance spectroscopy was conducted in the frequency ranging from 100 kHz to 1 Hz with a sampling rate of 10 points per second. The amplitude of the applied sinusoidal potential was 5.0 mV and the potential of + 0.25 V was limited to the formal potential of the redox couple $[Fe(CN)_6]^{3-/4-}$. The reported result for every DNA sensor in this experiment was the mean value of three parallel measurements. The electrochemical cell was housed in a specially shielded cage to reduce stray electrical noise during the measurements and all of the measurements were carried out at room temperature. An R(C(RW)) equivalent circuit (Nyquist plots) was used to fit the obtained impedance spectra.

Results and discussion

Synthesis of P/G_{ratios} composites

Graphene flakes with little defects were synthesized according to the already reported work.[34] As shown in Fig. 1(a) and 1(b), highly conductive and single-crystalline few-layer graphene flakes in size of several micrometers were clearly visible through SEM and TEM (ED pattern inset). XRD pattern (Fig. S1) of graphene confirmed its layered structures, in which the peak seen at 26.2° corresponds to the interspacing distance of the layers. No other phases were shown in the pattern, which means no impurity (i.e. lithium salt) was remained in the graphene solution to affect the behavior of the electrode and DNA adsorption. These graphene flakes can be easily dispersed in solution and dropped onto GCE to make a graphene-based sensor, but a problem was met because the graphene flakes tend to peel off the electrodes in DNA solution. However, if the graphene flakes are mixed with polyaniline which is a kind of conducting polymer, the problem can be solved. This should be attributed to stronger long-range π–π bonds and electrostatic interactions between graphene flakes and charged polyaniline. Fig. 1(c and d) shows the typical SEM and TEM images of PANI and graphene composite in the mass ratio of 1:1 (named $P/G_{1:1}$). It appears inter-stacking of flower-like polyaniline and few-layer graphene flakes. Polyaniline can work like “glue” sticking to graphene flakes. It can be suggested that the stability of graphene film would be improved by mixing graphene with positively charged polyaniline. The morphology of other composites of P/G with different mass ratio and morphology of the ssDNA/BSA modified electrode are shown in Fig. S2. As shown, the glue sticking PANI gets less, and the size also reduces, along with the decrease of the ratio of PANI to graphene. After the immobilization of ssDNA and BSA, the PANI/graphene composite (Fig. S2e) presents a rough surface appearance, due to the existence of immobilized pony-size biomass. The thickness of the film deposited was measured (Fig. S3.). As the result, the concentration of PANI would not affect the film thickness. The thicknesses of pure graphene and that in P/G composites were both about 3.2 nm. The P/G composites were

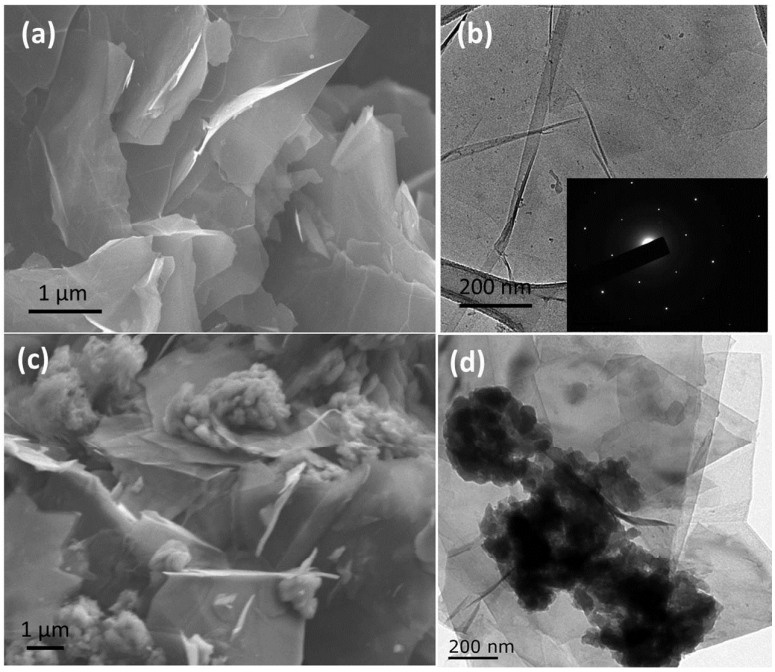

Figure 1. High quality of few-layer graphene nanosheets used for preparation of the hybrid of polyaniline and graphene platform. (a, b) The images of few-layer graphene nanosheets: SEM (a), TEM and inset electron diffraction pattern (ED) (b). (c, d) The hybrid of polyaniline and graphene.

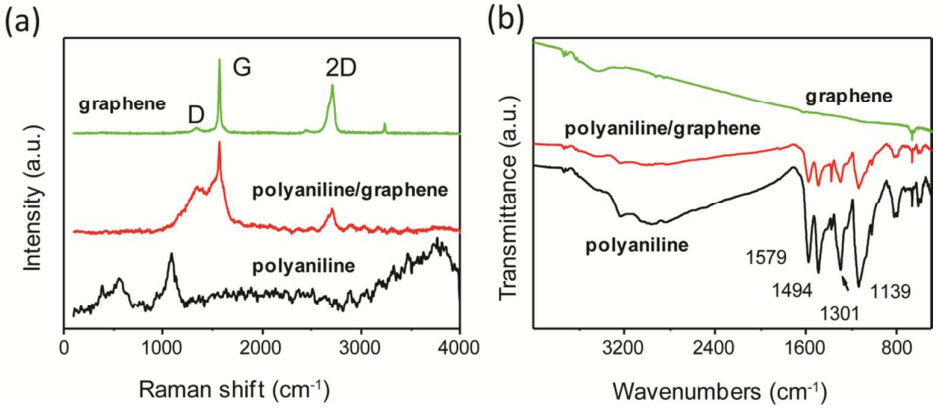

Figure 2. Spectroscopy characterizations of the hybrids of polyaniline/graphene compared with the component of few-layer graphene and polyaniline. (a) Raman (laser source of 488 nm), and (b) FTIR.

powerfully sonicated for more than 8 hours, and then centrifuged under a speed of 5000 rpm. Therefore, the average thickness of the film was controlled.

We took advantage of spectroscopy techniques to analyze the composites and compare the properties of each kind of composites. Little defects of graphene flakes were confirmed by Raman and FTIR spectra and these flakes are quite different from reduced graphene oxide, as shown in Fig. 2. Fig. 2a shows that in the hybrid the peaks of D band (~1350 cm^{-1}) and G band (~1570 cm^{-1}) of graphene were broadened and merged together, and the defective signal of D band increased much while the intensity of the 2D band decreased compared with those of pristine graphene. This may result from the coupling between graphene and polyaniline via strong long-range π–π and electrostatic interactions. FTIR spectra presented that the polyaniline features (1579 cm^{-1}, quinonoid ring vibration; 1494 cm^{-1} benzenoid ring vibration; 1301 cm^{-1} C-N stretching vibration; 1139 cm^{-1} C-H in-plain vibration) were kept in the hybrid. The absorbance of polyaniline in the hybrid is linearly related to its concentration in the hybrid (Fig. S4a). The increase of the mass ratio of polyaniline to graphene can improve the colloidal dispersion of graphene in water (Fig. S4b).

Construction of P/G_{ratios}-based DNA sensor

As the scheme for the synthesis procedures of the sensor presented (Fig. S5), the P/G_{ratios}-based DNA sensor was

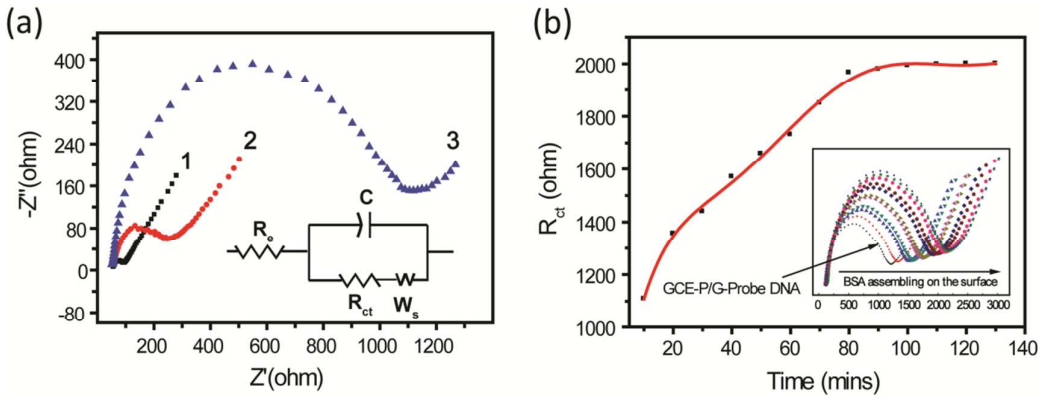

Figure 3. (a) Nyquist plots of the hybrid of polyaniline/graphene (the mass ratio 1:1, named $P/G_{1:1}$) based DNA sensor at various stages: (1) glassy carbon electrode (GCE), (2) GCE modified with $P/G_{1:1}$, and (3) GCE-P/G electrode immobilized by probe DNA. (b) Charge transfer resistance (R_{ct}) reflects the dynamic adsorption curve of BSA on the surface of the $P/G_{1:1}$–based sensor (Inset is Nyquist plots).All the impedance data were recorded in the presence of 10 mM of $K_{3/4}Fe(CN)_6$] and 3.5% of NaCl.

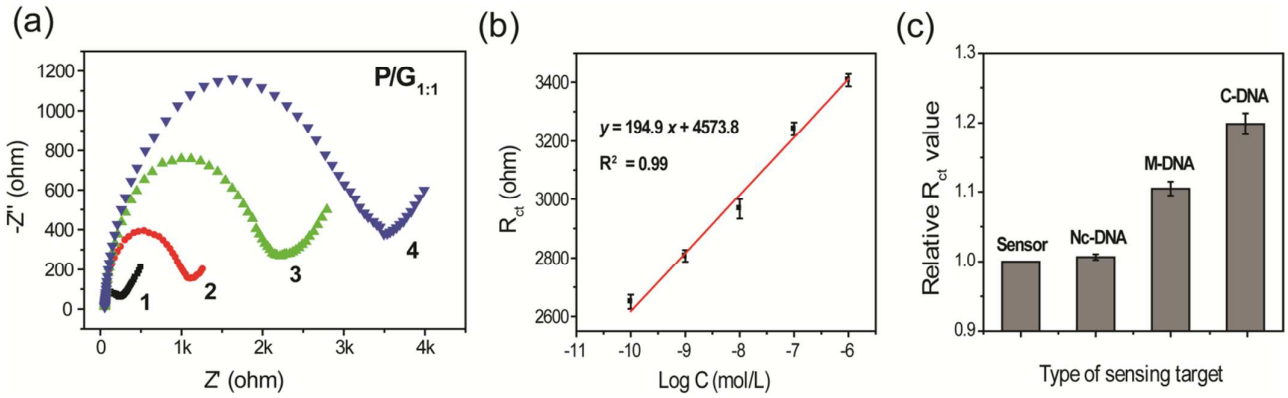

Figure 4. (a) Nyquist plots for polyaniline/graphene (when the mass ratio is 1:1, it is noted as $P/G_{1:1}$) based DNA sensor at various stages: (1) GCE-P/G (black line), (2) GCE-P/G-Probe DNA (red line), (3) GCE-P/G-Probe DNA-BSA (green line), and (4) GCE-P/G-Probe DNA-BSA-target DNA (blue line).The impedance was controlled by diffusion of the redox probe (of low frequencies) and by interfacial electron transfer (high frequencies). (b) Dependence of R_{ct} on the concentration of C-DNA for $P/G_{1:1}$–based sensor. (c) Histograms representing the relative detection values obtained for $P/G_{1:1}$–based sensor loaded with C-DNA, Nc-DNA, and M-DNA.

fabricated in three steps: firstly, bare GCE electrodes were polished and cleaned; secondly, P/G_{ratios} composites of a fixed mass ratio of polyaniline and graphene were deposited on the surface of GCE electrodes; and thirdly, the GCE modified with P/G_{ratios} were immersed in the solution of probe-DNA to allow the probe-DNA immobilize onto the electrode of GCE-P/G_{ratios}. It proves that high quality few-layer graphene flakes are of outstanding affinity to single stranded DNA owing to long range π-π interaction, and the single stranded DNA probe-DNA was thus immobilized onto the electrode GCE-P/G_{ratios}. Here, EIS, known as an effective method of probing into the features of surface-modified electrodes, was used to evaluate the electrochemical properties of the P/G_{ratios}-based DNA sensor in each step and came up with Nyquist plots as shown in Fig. 3. The curves of the Nyquist plots actually display two steps of electron movements: one is electron transfer, the semicircular portion of the curves, and the other is electron diffusion, the linear portion of the curves. The typical R(C(RW)) equivalent circuit, as shown in the inset of Fig. 3a, was used to fit EIS data and determine the electrical parameters in each step of the process and the concentration of the target DNA. The parameters of the circuit include Warburg element (W_s), electrolyte resistance (R_e), charge transfer resistance (R_{ct}) and constant phase element (C).[41] In this case, the non-specific adsorption of target DNA was taken into consideration due to the non-uniformity of P/G. To overcome this drawback, the sensor was immersed in bull serum albumin (2.5 g/L) to allow BSA self-assemble on the surface of P/G_{ratios}-based sensor. As shown in Fig. 3a, the semicircular domain of the curve of bare GCE electrode is of short diameter so that the R_{ct} of bare GCE electrode should be low. After GCE was modified with P/G, the diameter of the semicircle increased and was more specific. R_{ct} of modified electrode increases from 70 ohm to 220 ohm, which is also in a very small region, indicating P/G composites maintained the high electrical conductivity as pure graphene (Fig. S6). Due to the kinetics barrier between $[Fe(CN)_6]^{3-/4-}$ solution and the deposited probe, the R_{ct} of the GCE-P/G electrode increased dramatically from 220 ohm to 1,100 ohm

when the probe was deposited. Finally, with the self-assembling of BSA, R_{ct} continues to increase to a plateau because the adsorption of BSA on the surface of GCE-P/G electrode tends to saturate after 100 min (Fig. 3b).

EIS analysis of the P/G_{ratios}-based sensor

EIS allows analyzing interfacial changes originating from bio-recognition events on electrode surfaces through the capacitance and interfacial electron transfer resistance of the conductive or semi-conductive electrodes. To test the sensitivity and selectivity of the resulting P/G_{ratios}-based electrochemical DNA sensor, complementary DNA sequences (C-DNA), non-complementary DNA sequences (Nc-DNA) and mutant DNA sequences (M-DNA) were used as targeted DNA for the hybridization of the P/G_{ratios}-based DNA sensor. Usually, double-stranded DNA (dsDNA) and single-stranded DNA (ssDNA) possessed different linking affinities to the graphene-based substrate. Generally, the nitrogenous bases in ssDNA readily formed π-π bond stacking with the hexagonal units of graphene while dsDNA was less approachable to graphene due to the shield of the nitrogenous bases in double-helix structure.

It is generally accepted that the formed dsDNA escapes from the surface of DNA sensor and R_{ct} decreases as the concentration of C-DNA increasing when C-DNA is hybridized. However, this work illustrates that R_{ct} exhibits a positive linear relationship with the concentration of C-DNA in the range of 100 pM to 1 μm (Fig. 4a, b). That is, hybridized dsDNA remained on the surface of the sensor, which was quite different from the reported works.[30] Without BSA's self-assembling on the surface of P/$G_{1:1}$-based sensor, we obtained the similar results of the reported work[30] as shown on the Fig. S7. The reverse mechanism of C-DNA detection involved to the self-assembling of BSA is going to be discussed later. Fig. 4c is the R_{ct} of C-DNA, Nc-DNA and M-DNA (divided by the R_{ct} of P/G_{ratios}-based sensor) detected by P/$G_{1:1}$-based sensor. It's not hard to notice that R_{ct} changed only subtly after DNA sensor was met with Nc-DNA, which means that dsDNA wasn't effectively formed in this situation. As to M-DNA's hybridization, the R_{ct} value is much lower than that of C-DNA and this variation seems apparent in Fig. 4c. This finding is important because it proves P/$G_{1:1}$-based sensor's capability of discriminating single nucleotide polymorphisms (SNP) and meanwhile inspires a new route to apply P/G composites.

The exploration of the new route is based on the influence of the P/G mass ratios on the performance of the DNA sensors, which means that the authorial research group attempts to build a dynamic DNA sensor with changeable mass ratios of P/G to widen its detection range and they decided that this kind of DNA sensor should be named as P/G_{ratios}-based DNA sensors. The mass proportions of polyaniline and graphene varied from 1:1, 1:2, 1:10, 1:20 to 1:100. Correspondently, the synthesized composites were marked as P/$G_{1:1}$, P/$G_{1:2}$, P/$G_{1:10}$, P/$G_{1:20}$ and P/$G_{1:100}$. All of these P/G_{ratios} composites were employed to fabricate corresponding P/G_{ratios}-based sensor through the same procedure. The performance of P/G_{ratios}-based sensor was evaluated by the detection of C-DNA, as shown in Fig. 5. As one can see in Fig. 5a, the sensitivity of P/G_{ratios}-based sensor is improved when the mass ratio of polyaniline to graphene decreases, and the sensor's linear detection range of C-DNA concentration changes from [10^{-12}, 10^{-8}] mol/L to [10^{-14}, 10^{-10}] mol/L. Meanwhile, the slope of the curve of R_{ct} changes from positive 194.4 to negative 48.8 when the mass ratio of P/G changes from 1/1 to 1/100 (Fig. 5b), which indicates that dsDNA, the result of hybridization of target ssDNA to probe ssDNA, prefers to remain on the sensor surface when the mass ratio is higher than 1/10 while tends to release when the mass ratio is lower than 1/20. Then a conclusion is made that the ratio of 1/10 and 1/20 can be seen as the critical values when the slope angle of R_{ct} is close to 0, as readers can see in the Fig. 5a. That is, R_{ct} didn't change as the concentration of C-DNA increased from 0.01 pM to 1 uM in the case of P/$G_{1:20}$-based DNA sensor, which is apparently not scientific, and so the concentration of C-DNA cannot be discriminated by P/$G_{1:20}$-based DNA sensor.

Compared with P/$G_{1:1}$-based sensor, P/$G_{1:100}$-based sensor was also employed to detect M-DNA, Nc-DNA and C-DNA and the results seemed reversed to those of P/$G_{1:1}$-based sensor if Fig. 4c is compared with Fig. 6c. In terms of the hybridization of C-DNA and M-DNA, the R_{ct} of P/$G_{1:100}$-based sensor tended

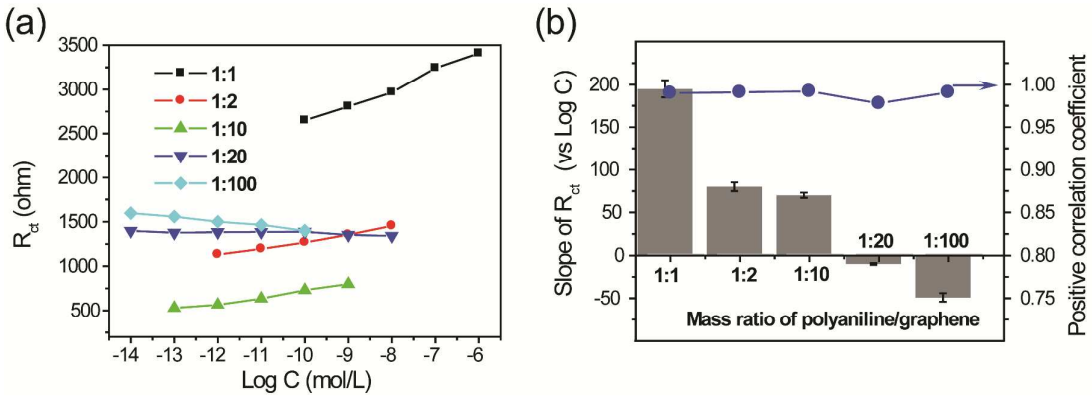

Figure 5. The plot of R_{ct} against the logarithm of the concentrations (logC) of the detection range of the C-DNA for polyaniline/Graphene hybrids with various mass ratios. (a) The linear relationship of R_{ct} and logC at various ratio of polyaniline/graphene. (b) The tendency of R_{ct} changed with mass ratio of polyaniline/graphene, which indicates selectivity.

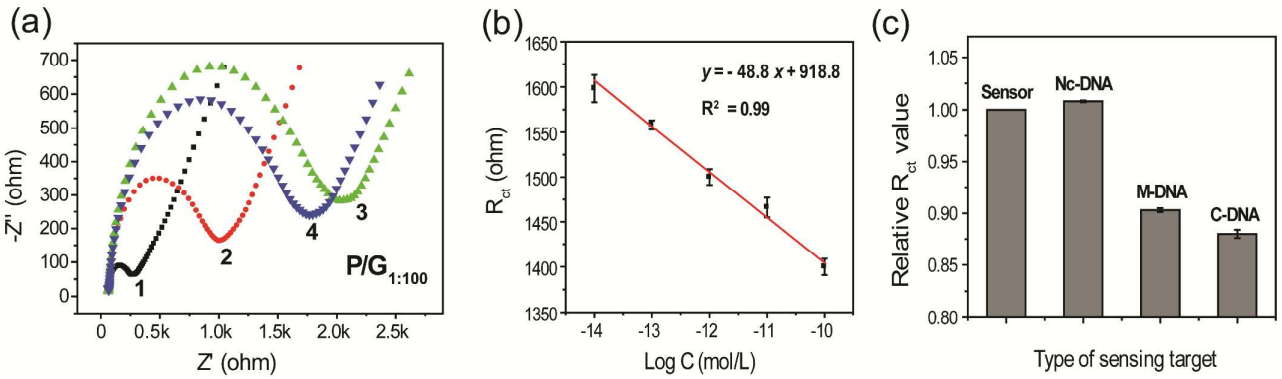

Figure 6. (a) Nyquist diagrams for polyaniline/graphene-based (the mass ratio 1:100, named P/$G_{1:100}$) sensor loaded on GCE at various stages. P/$G_{1:100}$ (1, black line), P/$G_{1:100}$-Probe DNA (2, red line), P/$G_{1:100}$-Probe DNA-BSA (3, green line), and P/$G_{1:100}$-Probe DNA-BSA-Target DNA(4, blue line). (b) Histograms representing the relative R_{ct} values obtained with the different oligonucleotides. (c) Histograms representing the relative detection values obtained for P/$G_{1:100}$–based sensor loaded with C-DNA, Nc-DNA, and M-DNA.

Table 1 Performance comparisons on analogical sensors of our work with reported ones recently

Main material	Detectingrange	LOD	Method	Literatures
Graphene/Gold	1 pm ~ 1 μm	1 pm	DPV	Pandian et al.[42]
Organic semiconductor	100 pm ~ 1 μm	100 pm	Transistors	Bonfiglio et al.[43]
Nano-gold	0.1 pm ~ 100 pm	0.1 pM	ECL	Zhang et al.[44]
rGO/ Polyaniline	1 fm ~ 10 nm	0.25 fm	EIS	Jiao et al.[30]
Graphene/ Aminopyrene	1 pm ~ 10 nm	0.45 pm	EIS	Wang et al.[45]
P/$G_{1:1}$- P/$G_{1:100}$	0.1 pm ~ 1 μm	0.01 pm	EIS	this work

to decrease, which also means the results of the hybridization of target DNA, dsDNA, were releasing off from the P/$G_{1:100}$-based sensor surface. The R_{ct} of Nc-DNA remained high and almost same as that of the DNA sensor, that is, on the one hand the initial R_{ct} of P/$G_{1:100}$-based sensor was larger than that of M-DNA and C-DNA; and on the other hand, Nc-DNA nearly did not hybridize with the probe-DNA. All these results actually echoed the effect of P/G's mass ratio illustrated in Fig. 4. However, it should be noted that the P/$G_{1:100}$-based sensor did not perform well on discriminating SNP. As shown in Fig. 6c, the R_{ct} obtained from detecting M-DNA was just 2.6% higher than that obtained from detecting C-DNA. It can be suggested that the hybridization of probe DNA and single base mismatched DNA would also form dsDNA-like DNA polymers. As a result, the ds-DNA would leave from the surface of sensor and lead to the decrease of R_{ct}.

It is worth noting that the newly proposed sensor breaks out the traditional idea that one sensor should only be equipped with a fixed ratio of polyaniline to graphene, but encourages taking advantage of composites of P/G in different ratios to strengthen the functions of sensors. For example, P/G_{ratios}-based sensor won't be able to discriminate the concentration of C-DNA in a wide range from 0.01 pM and 1 μM when the ratio of polyaniline to graphene is settled as a specific number. However, when the ratio of P/G is allowed to change, the whole range from 0.01 pM and 1 μM for the concentration of C-DNA became testable. Compared with the reported works, the dynamic P/G_{ratios}-based sensor shows great advantages over the analogical DNA sensor developed since 2012, as listed in Table 2. Our P/G_{ratios}-based sensor succeeded to reduce LOD to as low as 0.01 pM while widen the detecting range to be from 0.01 pM to 1 μM.

Except being excited with the results in terms of the influence of varied mass ratio of P/G, we continued to experiment on the impact of the conjugation of P/G composites in different ratios and BSA on the performance of P/G_{ratios}-based sensor. To further explore and elucidate the mechanism and anomalism in this field, pure polyaniline and pure graphene (prepared by the method of electrochemical reduction of graphene oxide) were employed to modify GCE and construct sensors. The electrochemical impedance spectroscopy was also employed to monitor the process in each construction step of pure polyaniline and graphene sensor, as shown in Fig. 7. When the polyaniline-modified GCE electrode was immersed into 10 μM probe-DNA solution for 4 hours, there were no significant change of the value of R_{ct}, which illustrates that few probe-DNA interacted with polyaniline. However, when GCE electrode was modified with the composites of polyaniline and graphene and then immersed into probe-DNA for 1 hour, the value of R_{ct} changed remarkably. Such response should be in the result of π-π stacking interaction between graphene and probe-ssDNA.

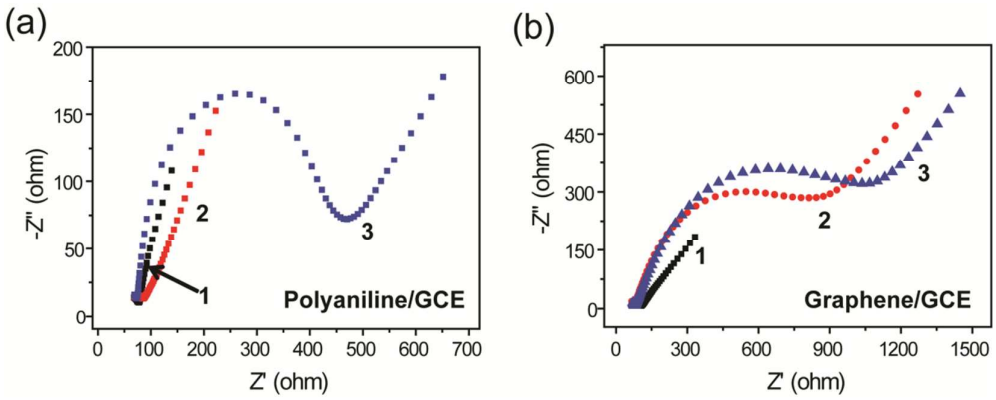

Figure 7. Nyquist diagrams in same frequencies range after each step of different components immobilization on polyaniline (a) and graphene (b) deposited on GCE. (a) Nyquist diagrams of polyaniline (1, black line), polyaniline-probe ssDNA (2, red line). polyaniline-probe ssDNA-BSA (3, blue line). (b) Nyquist diagrams of graphene (1, black line), graphene-probe ssDNA (2, red line), graphene-probe ssDNA-BSA (3, blue line).

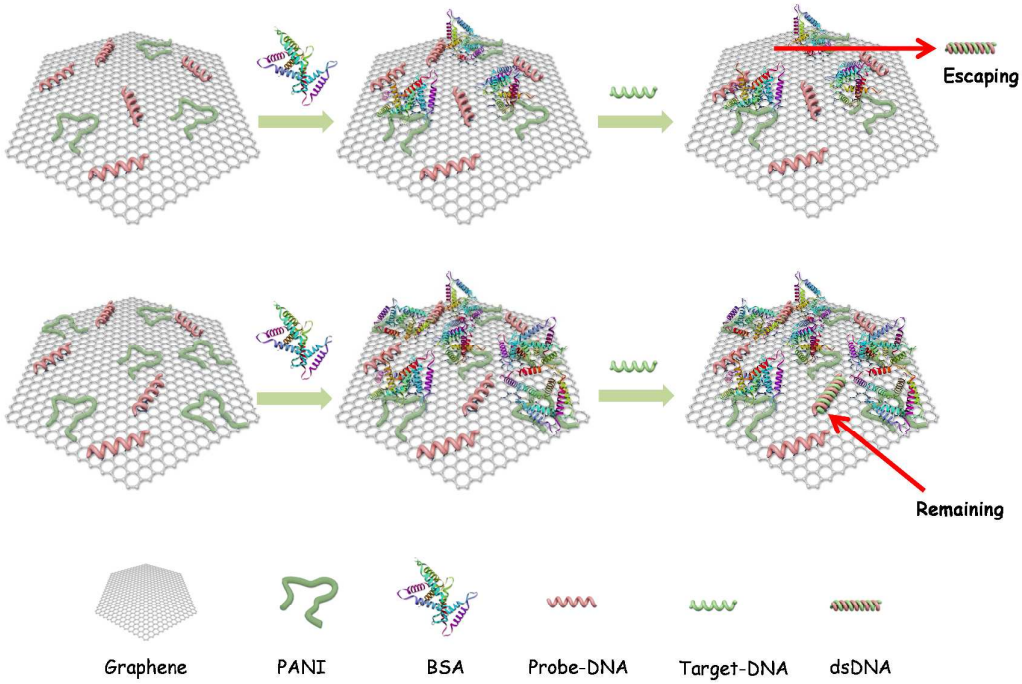

Scheme 1. Schematic illustration of the experimental protocol. The platform can easily load the probe ssDNA and the detection mechanism is affected by the ratio of polyaniline and graphene (P/G). (above) ds-DNA releases from the platform when the mass ratio of P/G is less than 1/20, (below) ds-DNA remains on the platform when the ratio of P/G is larger than 1/10.

Thus, it proved that the probe-ssDNA and graphene were united by P/G-based sensor. The R_{ct} enhanced when BSA assembled on polyaniline electrode (Fig. 7a) while only slightly changed when BSA was attached on graphene electrode (Fig. 7b), which suggested that BSA is easier to be adsorbed by polyaniline than graphene. This is reasonable since polyaniline has rich charged groups that can attract protein. To further demonstrate this, the zeta potential of ss-DNA, BSA modified P/G composites were measured, as shown in Fig. S8. The zeta potentials decreased with the mass ratio of polyaniline to graphene increase. This suggested more negatively charged BSA was aggregated on the P/G composite particles. The results fairly correspond with the EIS analysis. As a result, when polyaniline's ratio rises in the composites of P/G, there should be more BSA adsorbed to the surface of P/G_{ratios}-based sensor. This actually sheds light on the explanation for the many results in this paper. Firstly, no matter whether the DNA is probe-ssDNA or dsDNA in the result of hybridization, there exists electrostatic interaction between DNA and polyaniline or/and BSA. It is believable that the electrostatic interaction plays an essential part in maintaining DNA on the surface of the sensor. Secondly, both probe ssDNA and dsDNA would interact with graphene through π-π stacking attraction, but the π-π stacking interaction between graphene and dsDNA is in fact weakened due to the shield of the nitrogenous bases which is of double-helix structure. And the strength of π-π

stacking interaction becomes so weak in the case of dsDNA that this strength could be neglected in terms of its influence on the position of dsDNA to the sensor's surface. Different with electrostatic interaction and π-π stacking interaction, both of which maintain dsDNA on the surface of the sensor, Brownian motion is the one that stands on their opposite side and helps dsDNA escape from the sensor's surface. Since π-π stacking interaction could barely influence the position of dsDNA, whether it would remain or release from the surface of P/G_{ratios}-based sensor should be a result of the competition between Brownian motion and the electrostatic interaction, as shown in Scheme 1. The electrostatic force of the interaction among dsDNA, polyaniline and BSA should be increasingly attenuated with the decrease of the ratio of polyaniline to graphene. The dsDNA releases from the sensor's surface in the influence of Brownian motion when the ratio of P/G is as low as 1:100; while dsDNA stays on the surface of sensor when the ratio is high as 1:1. When the ratio reaches 1:20, there are hardly any change of R_{ct} detected, which means that there should be a balance realized between Brownian motion and electrostatic interaction. In this case, it becomes not authentic to use the sensor to determine the concentration of target ssDNA directly, let alone single nucleotide polymorphisms. In addition, it is understandable that the sensitivity of sensor is in direct proportion to the concentration of graphene.

Real sample analysis

As a biosensor, it is extremely important to verify its application with extracted DNA from real samples. In Fig. 8, EIS measurements show the signals obtained with the pUC19 DNA(target, i.e, real sample). It was observed that in the presence of target the R_{ct} value of $P/G_{1:1}$ sensor (Fig. 8a) was increased and the R_{ct} value of $P/G_{1:100}$ sensor (Fig. 8b) was decreased, which confirmed the occurrence of hybridization. It was also observed that the cyclic voltammetry curve peak of $P/G_{1:1}$ sensor (inset of Fig. 8a) decreased while the peak of $P/G_{1:100}$ sensor (inset of Fig. 8b) increased, indicating the formed dsDNA molecule remain or release from the surface. In Fig. 8c and 8d, the R_{ct} values of the sensors for synthetic oligonucleotides were compared with that for extracted DNA in the same concentration. As seen in Fig. 8c, the relative R_{ct} value of $P/G_{1:1}$ sensor for real sample was significantly higher than that for synthetic oligonucleotides. This can be suggested that longer target oligonucleotides would generate more severe electron transfer effect. And as shown in Fig. 8d, with the $P/G_{1:100}$ sensor, the decrement in R_{ct} value was slightly lower for real sample detection than that for synthetic oligonucleotides detection. Kalantari et al. reported that the target length (38, 107, 1788 and 2907 base pairs) can contribute to changes in the hybridization signal, [46] which was in good agreement with the P/G sensor.

Conclusions

In conclusion, we designed a dynamic P/G_{ratios}-based DNA sensor capable of detecting C-DNA in a range from 0.01 pm to 1 μm through changing ratios of polyaniline to graphene. Moreover, SNPs are also detectable for such sensors. This work also explores the reasons behind the dynamic relationship between R_{ct} and ratios of P/G, and concludes that

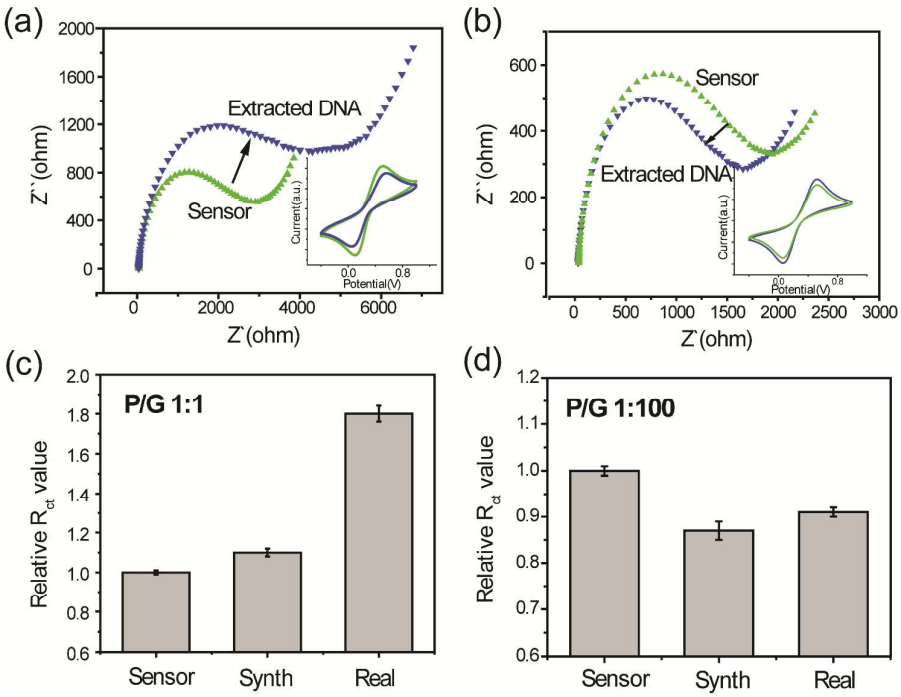

Figure 8. Nyquist diagrams of $P/G_{1:1}$ (a) and $P/G_{1:100}$ (b) sensors for the pUC19 DNA detection, inset was the corresponding cyclic voltammetry curve. And the relative R_{ct} value of the $P/G_{1:1}$ (c) and $P/G_{1:100}$ (d) sensors for synthetic/real sample DNA in the same concentration.

electrostatic interaction among dsDNA, BSA and polyaniline, and Brownian motion should be the decisive forces for dsDNA's remaining on or releasing off the surface of the sensor. That is, one is able to control the movement tendency of dsDNA by changing the proportion of polyaniline in the composites, which is helpful for the fabrication of novel biosensors. And on this basis we proposed that the increasing response of charge transfer resistance should result from dsDNA's remaining on the surface with much polyaniline while the decreasing response should be assigned to dsDNA's releasing off the sensor with dominative graphene.

Acknowledgements

We gratefully acknowledge the support for this work from Fundamental Research Funds for the Central Universities (S13JB00200, 2015JBM102), the National Natural Science Foundation of China (Grants 11079010, 21373255), the Hundred Talent Program of the Chinese Academy of Sciences (2013SCXQT01) and the Key Laboratory of Carbon Materials (KLCMKFJJ1401).

Notes and references

‡*Corresponding authors.
Tel: 86-10-51688577. E-mail: dkjian@bjtu.edu.cn (K.J. Ding).
Tel: 86-351-4040407. E-mail: wangjz@sxicc.ac.cn (J.Z. Wang).

1. L. Feng, Y. Chen, J. Ren and X. Qu, *Biomaterials*, 2011, **32**, 2930-2937.
2. X. Y. Wang, A. Gao, C. C. Lu, X. W. He and X. B. Yin, *Biosens. Bioelectron.*, 2013, **48**, 120-125.
3. K. Deng, Y. Xiang, L. Zhang, Q. Chen and W. Fu, *Anal. Chim. Acta*, 2013, **759**, 61-65.
4. M. Trojanowicz, *Electrochem. Commun.*, 2014, **38**, 47-52.
5. D. Sidransky, *Science*, 1997, **278**, 1054-1059.
6. M. Wang, C. Sun, L. Wang, X. Ji, Y. Bai, T. Li and J. Li, *J. pharm. biomed.anal.*, 2003, **33**, 1117-1125.
7. Q. Wang, J. Lei, S. Deng, L. Zhang and H. Ju, *Chem Commun (Camb)*, 2013, **49**, 916-918.
8. L. Wang, E. Hua, M. Liang, C. Ma, Z. Liu, S. Sheng, M. Liu, G. Xie and W. Feng, *Biosens. Bioelectron.*, 2014, **51**, 201-207.
9. A. Florea, Z. Taleat, C. Cristea, M. Mazloum-Ardakani and R. Săndulescu, *Electrochem. Commun.*, 2013, **33**, 127-130.
10. A.-N. Kawde, M. C. Rodriguez, T. M. H. Lee and J. Wang, *Electrochem.Commun.*, 2005, **7**, 537-540.
11. R. Tong, L. Yala, T. M. Fan and J. Cheng, *Biomaterials*, 2010, **31**, 3043-3053.
12. Y. Fu, C. Zou, L. Bu, Q. Xie and S. Yao, *ACS Appl. Mater. Interfaces*, 2013, **5**, 934-939.
13. K. Maehashi, T. Katsura, K. Kerman, Y. Takamura, K. Matsumoto and E. Tamiya, *Anal. Chem.*, 2007, **79**, 782-787.
14. A. R. Ruslinda, V. Penmatsa, Y. Ishii, S. Tajima and H. Kawarada, *Analyst*, 2012, **137**, 1692-1697.
15. W. Song, H. Li, H. Liu, Z. Wu, W. Qiang and D. Xu, *Electrochem. Commun.*, 2013, **31**, 16-19.
16. H. A. Ho and M. Leclerc, *J. Am. Chem. Soc.*, 2004, **126**, 1384-1387.
17. Y. C. Lim, A. Z. Kouzani and W. Duan, *J Biomed. Nanotechnol.*, 2010, **6**, 93-105.
18. J. H. An, S. J. Park, O. S. Kwon, J. Bae and J. Jang, *ACS Nano*, 2013, **7**, 10563-10571.
19. L. Jiang, J. Qian, X. Yang, Y. Yan, Q. Liu and K. Wang, *Anal. Chim. Acta*, 2014, **806**, 128-135.
20. K. S. Novoselov, V. I. Fal'ko, L. Colombo, P. R. Gellert, M. G. Schwab and K. Kim, *Nature*, 2012, **490**, 192-200.
21. X. Yan, J. Chen, J. Yang, Q. Xue and P. Miele, *ACS Appl. Mater. Interfaces*, 2010, **2**, 2521-2529.
22. L. Wang, J. Zhu, L. Han, L. Jin, C. Zhu, E. Wang and S. Dong, *ACS Nano*, 2012, **6**, 6659-6666.
23. O. Akhavan, E. Ghaderi and R. Rahighi, *ACS Nano*, 2012, **6**, 2904-2916.
24. S. R. Ryoo, J. Lee, J. Yeo, H. K. Na, Y. K. Kim, H. Jang, J. H. Lee, S. W. Han, Y. Lee, V. N. Kim and D. H. Min, *ACS Nano*, 2013, **7**, 5882-5891.
25. Y. Wang, Z. H. Li, J. Wang, J. H. Li and Y. H. Lin, *Trends Biotechnol.*, 2011, **29**, 205-212.
26. L. Tang, Y. Wang, Y. Liu and J. Li, *ACS nano*, 2011, **5**, 3817-3822.
27. A. Bonanni, C. K. Chua, G. Zhao, Z. Sofer and M. Pumera, *ACS nano*, 2012, **6**, 8546-8551.
28. S. Grützke, S. Abdali, W. Schuhmann and M. Gebala, *Electrochem. Commun.*, 2012, **19**, 59-62.
29. A. Bonanni and M. Pumera, *ACS Nano*, 2011, **5**, 2356-2361.
30. T. Yang, Q. Li, X. Li, X. Wang, M. Du and K. Jiao, *Biosens. Bioelectron.*, 2013, **42**, 415-418.
31. A. Li, F. Yang, Y. Ma and X. Yang, *Biosens. Bioelectron.*, 2007, **22**, 1716-1722.
32. Y. Xu, H. Cai, P. G. He and Y. Z. Fang, *Electroanalysis*, 2004, **16**, 150-155.
33. R. Ghosh, A. Midya, S. Santra, S. K. Ray and P. K. Guha, *ACS Appl. Mater. Interfaces*, 2013, **5**, 7599-7603.
34. J. Wang, K. K. Manga, Q. Bao and K. P. Loh, *J. Am. Chem. Soc.*, 2011, **133**, 8888-8891.
35. L. A. Tang, J. Wang and K. P. Loh, *J. Am. Chem. Soc.*, 2010, **132**, 10976-10977.
36. Y. F. Lin, C. H. Chen, W. J. Xie, S. H. Yang, C. S. Hsu, M. T. Lin and W. B. Jian, *ACS Nano*, 2011, **5**, 1541-1548.
37. J. Singh, A. P. Bhondekar, M. L. Singla and A. Sharma, *ACS Appl. Mater. Interfaces*, 2013, **5**, 5346-5357.
38. D. Zhai, B. Liu, Y. Shi, L. Pan, Y. Wang, W. Li, R. Zhang and G. Yu, *ACS Nano*, 2013, **7**, 3540-3546.
39. X. Wang, T. Yang, X. Li and K. Jiao, *Biosens. Bioelectron.*, 2011, **26**, 2953-2959.
40. Y. Hu, T. Yang, Q. Li, Q. Guan and K. Jiao, *Analyst*, 2013, **138**, 1067-1074.
41. E. Casero, A. M. Parra-Alfambra, M. D. Petit-Domínguez, F. Pariente, E. Lorenzo and C. Alonso, *Electrochem. Commun.*, 2012, **20**, 63-66.
42. K. Jayakumar, R. Rajesh, V. Dharuman, R. Venkatasan, J. H. Hahn and S. K. Pandian, *Biosens. Bioelectron.*, 2012, **31**, 406-412.
43. S. Lai, M. Demelas, G. Casula, P. Cosseddu, M. Barbaro and A. Bonfiglio, *Adv. Mater.*, 2013, **25**, 103-107.
44. W. Yao, L. Wang, H. Wang, X. Zhang, L. Li, N. Zhang, L. Pan and N. Xing, *Biosens. Bioelectron.*, 2013, **40**, 356-361.
45. L. Q. Luo, Z. Zhang, Y. P. Ding, D. M. Deng, X. L. Zhu and Z. X. Wang, *Nanoscale*, 2013, **5**, 5833-5840.
46. R. Kalantari, R. Cantor, H. Chen, G. Yu, J. Janata and M. Josowicz, *Anal. Chem.*, 2010, **82**, 9028-9033